STSM REPORT

COST STSM Reference Number: COST-STSM-BM1205—15533

STSM Grantee: Prof **Vitomir Milanovic**

STSM title: Modelling of THz quantum cascade lasers for applications in biomedical imaging

Home Institution: School of Electrical Engineering, University of Belgrade, Serbia

Host Institution: School of Electronic and Electrical Engineering, University of Leeds, UK

Host: Dr Dragan Indjin

STSM period: 1 November 2013 – 30 November 2013

STSM purpose: Strenghten collaboration between groups and open new direction in modelling and optimisation of second oreder and self-mixing effects in quantum-cascade lasers

STSM REPORT

During my visit in Leeds, we (members of group in Leeds and I) were worked on and prepared for submission a joint journal paper on optimization of quatum cascade laser (QCL) in mid-infrared spectral range. In this paper, we have described a procedure for the design of a GaInAs-AlInAs-based QCL with optimized optical nonlinearity capability. The technique has no restrictions regarding the number of the optimization parameters or material composition, and demonstrates high optimization abilities. The designs were evaluated by modeling the carrier dynamics using the full self-consistent approach extended *with photon density equations*, and the reference design modeling and corresponding calculations show excellent agreement with experimental results. The described procedure is applicable to various active region designs and will be used in further work for other wavelength ranges, especially terahertz range. The developed method will also be an excellent ground for proper modeling of other second-order effects in QCLs very relevant for current applications in imaging, spectroscopy and material characterization.

Furthermore, we worked on dynamical and phenomenological modeling of bound –to – continuum (BTC) QCLs experiencing optical feedback. Firstly, we look at existing steady state model for our BTC THz QCLs and discussed how to include optical feedback via perturbation of the photon density. The starting point for developing our model are papers: Y.

Petitjean et al, IEEE J. Selected Topics Quant. Electron., **17**, 22, 2011 and M. K. Halder, IEEE J. Quantum Electron., **41**, 1349, 2005. Based on the paper by A. Hugi et al, Semcond. Sci. Technol., **25**, 1, 2010 , we preformed development of basic feasibility study how to model thermal injection of carriers and incorporate feedback via optical reinjection of radiation into laser cavity following pioneering work by R. Lang and K. Kobayashi (IEEE J. Quantum Electron., **16**, 347, 1980).

Our model assumes existence of two effective levels only: upper and lower laser levels, with corresponding injection efficiency, taken from full QCL model without feedback. Therefore, this problem consists of system of four first order nonlinear differential equations. Solving this system of differential equations we would calculate electron concentrations on upper and lower level. Relative changes of this concentrations approximately cause changes in output voltage. This change of voltage may be experimentally observed. Also, we analyzed possibility of optimization of this effect by method of genetic algorithm. We made a clear plan for further collaboration, and as starting point numerical simulation will be performed in Belgrade, with an aid of PhD student who is a member of Belgrade group. Further joint journal publications are expected from this collaboration.

The Quantum Electronics group in the School of Electronic and Electrical Engineering, University of Leeds has great experience in research of QCLs with over hundred papers in highly ranking international journals. Collaboration with Leeds' group and in particular with Dr Dragan Indjin and Dr Zoran Ikonic during this STSM visit was very intensive, useful and potentially highly beneficial to Belgrade's group, in order to complete development of the model for THz QCL under the optical feedback. On the other hand, group from Leeds, in our opinion, will gain a benefit of implementing optimization techniques developed in Belgrade where our group has great experience and track record of many published papers.

STSM outcome form STSM application number	Home institution & country	Host institution & country	BM1205 WG	Objective of the collaboration	Results of the collaboration
COST-STSM-BM1205—15533	**University of Belgrade, Serbia**	**University of Leeds, UK**	**WG2/WG3 THz/MIR**	**Developement of models for second order effects and self-mixing in QCLs**	**Develpoed model for SHG QCL optinistation and basic model for Self-mixing in QCLs**

I acknowledge that the described short term scientific mission was successfully carried out in the conditions here specified. Collaborations between partners was further developed and in the first instance, a joint journal paper was submitted to Journal of Applied Physics.

Leeds, 20 December 2013

Dragan Indjin

Dr Dragan Indjin
Reader in Optoelectronics and Nanoscale Electronics,
Institute of Microwaves and Photonics
School of Electronic and Electrical Engineering
University of Leeds, LS2 9JT, UK

Quantum Cascade Lasers with Second Harmonic Generation Optimized Active Regions

A. Gajić[1,2,a)], J. Radovanović[1], V. Milanović[1], D. Indjin[3], Z. Ikonić[3]

[1] *School of Electrical Engineering, University of Belgrade, Bulevar kralja Aleksandra 73, 11120 Belgrade, Serbia*

[2]*Telekom Srbija, a.d., Takovska 2, 11000 Belgrade, Serbia*

[3]*School of Electronic and Electrical Engineering, University of Leeds, Leeds LS2 9JT, UK*

Abstract. We present a computational model developed for the optimization of the second order optical nonlinearities in GaInAs/AlInAs quantum cascade laser (QCL) structures. It is based on the implementation of the Genetic algorithm (GA) with the purpose of determining a set of design parameters that satisfy predefined conditions, leading to an enhancement of the device output characteristics. In the following step, upon obtaining the optimized structure, carrier transport and the power output of the structure were calculated by self-consistently solving the system of rate equations for carriers and photons. Both stimulated and simultaneous double photon absorption processes that occur between the second harmonic generation (SHG) -relevant levels are incorporated into the rate equations, and material-dependent effective mass, as well as band nonparabolicity, are taken into account. The developed method is general, and can be applied to any higher order effect which requires photon density equitation included. Specifically, we have addressed the optimization of the active region of a double quantum well (QW) $In_{0.53}Ga_{0.47}As/Al_{0.48}In_{0.52}As$ structure and presented the output characteristics of the designed optimized structure.

PACS: 42.55.Px Semiconductor lasers; laser diodes, 42.65.Ky Frequency conversion; harmonic generation, including higher-order harmonic generation, 73.21.Fg Quantum wells

I. INTRODUCTION

The wide range of emission wavelengths, as well as room temperature operation, have marked quantum cascade lasers (QCLs) as one of the most sophisticated and reliable light sources in the infrared and terahertz region of the electromagnetic spectrum[1 2 3 4 5 6 7]. Their fast development led to high performance devices which have been commercialized by several companies, such as Nanoplus and Alpes Lasers, in the past decade.

a) Electronic mail: aleksandragaj@telekom.rs

QCLs are one of the greatest examples of how intersubband transitions can be tailored to suit a particular purpose simply by changing the material composition and layer thickness of the constituent semiconductor materials, thus engineering the electronic energy states and wave functions[8] [9]. Beside their linear optical properties, resonant intersubband transitions can also be utilized as strongly nonlinear oscillators, enabling huge nonlinear optical susceptibilities to take place[10]. These optical nonlinearities can have a vast range of possible applications due to the capability of changing the frequency of the fundamental laser source[11] [12]. The nonlinear susceptibility represents an intrinsic property of a specific material system, which basically means that every media can provide optical nonlinearities[13], but in most cases the effect is too weak to be observed or utilized. In order to enhance the interaction of photons, an optical medium with a large nonlinear susceptibility is required[14].

The existence of a systematic and precise modeling technique, which will enable a deeper insight of the physical processes occurring in these complex devices, is a prerequisite for the successful design of QCL structures. The inclusion of all relevant scattering mechanisms that take place in both the optically active and collector(extractor)/injector multi-quantum well (QW) regions of the QCL is essential for an accurate description of the carrier dynamics[15] [16].

In the work presented here, we will address the optimization of two-QW active region mid-infrared (MIR) QCLs[17] with respect to the resonant second-order susceptibility. The optimal potential profile that maximizes the product of dipole matrix elements relevant to $\chi^{(2)}$ associated with second harmonic generation (SHG) is obtained by employing the Genetic algorithm (GA). The output properties of the optimized structure are calculated by using the full self-consistent rate equation model, where subband carrier density and photon density equations are included[18] [19], and the results of the calculations predict a noticeable improvement of the targeted nonlinear optical susceptibility and consequently the nonlienar output power for the optimized design. Both, the reference and optimized device, are designed for fundamental and SHG laser emission at λ~9μm and λ~4.5μm, respectively.

II. THEORETICAL CONSIDERATIONS

A. Genetic Algorithm

Genetic Algorithms are a family of computational models created with the purpose of solving complex problems by mimicking the process of natural evolution. They represent

search heuristics used to generate solutions to optimization and search problems by a combination of selection, recombination and mutation[20].

GAs belong to a larger class of evolutionary algorithms (EA), which generate solutions using techniques inspired by nature, such as inheritance, mutation, selection, and crossover. An implementation of a genetic algorithm begins with a population of typically random chromosomes into which a potential solution to a specific problem is encoded. At each step, the genetic algorithm randomly selects individuals from the current population and uses them as parents to produce the children for the next generation. Over successive generations, the population "evolves" toward an optimal solution. The “fitness” of a solution is typically defined with respect to the current population.

Genetic algorithms are often viewed as function optimizers, although the range of problems to which they have been applied is quite broad. Of particular interest are applications to problems that are not well suited for standard optimization algorithms, entailing objective functions which are discontinuous, nondifferentiable, stochastic, or highly nonlinear.

The code used in this work[21] initializes a random sample of individuals with different parameters to be optimized using evolution via survival of the fittest. The selection scheme used is tournament selection with a shuffling technique for choosing random pairs for mating. The routine includes binary coding for the individuals, jump mutation, creep mutation, and the option for single-point or uniform crossover. Niching (sharing) and an option for the number of children per pair of parents have been added.

Since the optimization of the entire QCL structure would be extremely computationally demanding, we have focused on the optimization of the active region which we then seamlessly assimilate with the existing injector/collector design.

1. Active region optimization

Active regions in QCL have been designed in many ways, the number of constituent quantum wells varying from a single QW to ten coupled QWs or even superlattices[22]. However, a typical MIR design based on electron-longitudinal optical (LO) phonon depopulation mechanism, implies a minimum of three consecutive energy levels, with the radiative transitions occurring between the upper and lower laser levels, i.e. levels 3 and 2, while level 2 is quickly depleted of electrons by resonant LO phonon scattering into level 1.

The electrons are scattered into the upper laser level from the preceding injector region and, after the radiative transition occurs, are transferred to the collector (extractor) region via LO scattering from the lower laser levels. High-performance QCLs are also characterized by large optical dipole matrix elements for the 3-2 transitions, long upper laser level and short lower laser level lifetimes, as well as fast radiative transitions from the upper into the lower laser level.

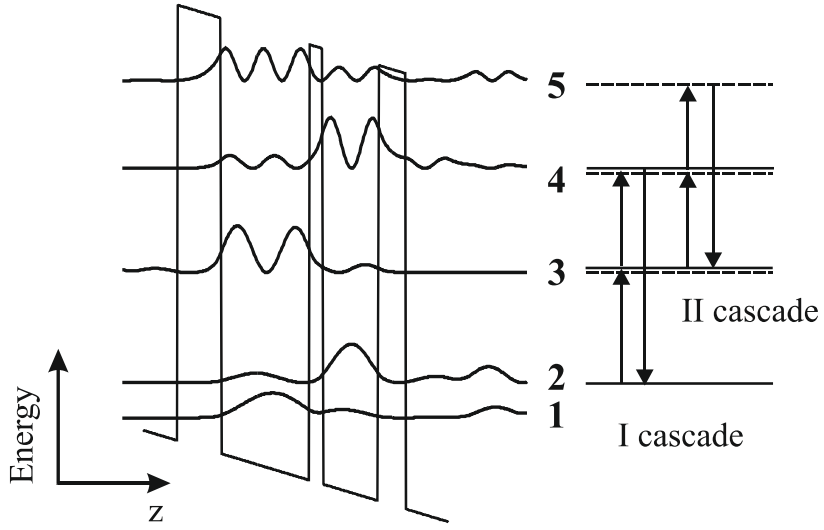

FIG. 1. Conduction band diagram and moduli squared of the essential wavefunctions of the reference structure, Ref. 17, active region; the SHG nonlinear cascades are indicated to the right of each active region. Cascades I (continuous line) and II (dashed line) extend over the levels 2-3-4 and 3-4-5, respectively.

A QCL structure capable of second harmonic generation contains another significant energy triplet, in which at least one energy level needs to be populated with free electrons in order for the structure to be able to generate radiative transitions and act as an efficient nonlinear converter. This sets an important design requirement, i.e. that the upper laser level needs to coincide with one of the levels in the nonlinear cascade. This is best illustrated in Fig. 1, which shows close-up details of the reference structure conduction band diagram and moduli squared of the active region essential wavefunctions. The SHG nonlinear cascades are indicated on the right of the active region. Cascades I (continuous line) and II (dashed line) extend over the levels 2-3-4 and 3-4-5, respectively.

In our optimization model, we start with the existing design (see Ref. 17) in which the active region consists of two coupled InGaAs quantum wells separated with an AlInAs barrier.

The optimization target function is chosen so to enable the maximization of the second order nonlinear susceptibility[23]:

$$\chi^{(2)}(2\omega) \approx \frac{2\pi e^3}{d\varepsilon_0}\left[\frac{M_{23}M_{34}M_{24}}{\gamma_{42}}\left(\frac{n_3-n_4}{\gamma_{43}}+\frac{n_3-n_2}{\gamma_{32}}\right)+\frac{M_{34}M_{45}M_{35}}{\gamma_{53}}\left(\frac{n_4-n_5}{\gamma_{54}}+\frac{n_4-n_3}{\gamma_{43}}\right)\right] \quad (1)$$

where M_{ij} is the dipole matrix element (DME) between levels i and j, γ_{ij} is the full width half maximum (FWHM) for transitions occurring between levels i and j, with the following values (Ref. 22): $\gamma_{42}= \gamma_{53}$=20meV, $\gamma_{43}= \gamma_{54}$=15meV and γ_{32}=10meV, n_i is the sheet electron density on the level i, and d represents the layers width.

Taking into account that $n_3 >> n_4$, n_5, as well as that the γ_{ij} values can be considered similar, it may be given in the following simplified form:

$$F_T = \left| M_{34} \cdot n_3 \left(M_{23} \cdot M_{24} \cdot \left(2 - \frac{n_2}{n_3} \right) - M_{45} \cdot M_{35} \right) \right| \quad (2)$$

From [Eq. (1)] we can see that $\chi^{(2)}$ is proportional to the product of the three optical dipole matrix elements $M_{23}M_{34}M_{24}$ for cascade I and $M_{34}M_{45}M_{35}$ for cascade II. The nonlinearity can be further enhanced by increasing this product while retaining the multiple resonances between levels.

The objective is to maximize the function F_T, given in equation (2), while at the same time the active region continues to match the existing injector/collector regions described in the reference (Ref. 17). The transition energies, ΔE_{21} and ΔE_{32}, defined by the LO phonon and transition energy, respectively, together with the transition energies between the levels constituting the cascades, ΔE_{54} and ΔE_{43}, should remain unchanged. While maintaining the energy differences, the shape of the wave functions can be modified by varying the potential profile in order to influence the parameters of interest in the calculation of the target function.

The parameter vector consists of layer thicknesses, which are only allowed to have non-negative values, and these are limited to 105 Å for wells and 30 Å for barriers. Additional constraints regarding the minimal value of the matrix element, as well as the upper laser level energy, which is set to fit the injector region, are also taken into account during the optimization process. The algorithm is tuned to encourage the selection of potential profiles that favor diagonal transitions, with the intention of increasing the upper laser level life times.

The existing injector/collector region is then added to the calculated optimized active region, which concludes the design process.

B. The self-consistent rate equation model

Once the optimized structure is obtained and its energies and wave functions are evaluated, we can extract its output characteristics by applying the full self-consistent rate equation modeling of the electron transport in a periodic QCL structure (Ref. 15) where this time photon density equations are included. An inclusion of equations describing single and double-photon stimulated emission processes will significantly add to the complexity of the numerical procedure and make the convergence of the system more challenging. However, this approach will provide with a more general optimization method which will be readily used in real-life applications of higher-order effects in QCLs we are developing now, see for example Ref. [24] [25] [26].

Let us look into a biased QCL structure with a large number of periods, each consisting of multiple quantum wells. In such a structure the energy spectrum is formally continuous, but to a very good approximation can be considered to consist of quasi-discrete states (resonances). For each of the periods within the structure we can identify an identical set of N states based upon the wave function localization properties. Electron scattering occurs between states within the same period as well as between states associated to different periods. However, the influence of the latter decreases as the wave function overlap lowers, so practically only the states belonging to neighboring periods interact significantly. Assuming an identical electron distribution in each period, one may consider some "central" period with its P nearest neighbours on either side, and write the scattering rate equations in the steady-state[27]:

$$\sum_{j=1,\,j\neq i}^{N} n_j W_{j,i} - n_i \sum_{j=1,\,j\neq i}^{N} W_{i,j} + \sum_{k=1}^{P} \sum_{j=1,\,j\neq i}^{N} \left[n_j \left(W_{j,i+kN} + W_{j+kN,i} \right) - n_i \left(W_{i+kN,j} + W_{i,j+kN} \right) \right] = 0 \qquad (3)$$

$$i \in \left(1, N^2 \left(2P^2 + 1\right) - N\right)$$

where $i+kN$ is the i-th state of the k-th neighbouring period, and $W_{i,j}$ is the total scattering rate from state i into state j. The first two sums in [Eq. (3)] are due to intra-period, while the third is a consequence of inter-period scattering. Since the number of total scattering rate

processes equals to $N^2(2P+1)$-N, in order to reduce the number of scattering rate processes necessary to calculate the electron distribution, we have introduced the "tight-binding" approximation[28] assuming that only the nearest neighbours interact, and set P=2.

In the model applied in this calculation, we can use a simplified form of [Eq. (3)], in which the number of relevant energy levels is restricted to five per QCL region (five in the optically active region, and five in each injector and collector/extractor regions), see Fig. 2. Adopting, for example, the notation and subband indexes given in Ref. 27, the injector and collector regions are represented with five energy levels each, subbands 1, 2, 3, 5 and 7 in the collector, and 8, 10, 11, 13 and 15 in the injector. The active region levels 14, 12, 9 and 6 are equally spaced with the energy intervals resonant to the lasing frequency. Level 4 represents the active region ground state which is located one LO phonon energy below the lower laser level in order to facilitate faster carrier extraction from the active QCL region into the following collector/injector region of the subsequent period, see Fig. 2.

The contribution of SHG resonant levels, i.e., 6-9-12 and 9-12-14 cascades, is reflected through both sequentially and simultaneously resonant intracavity two-photon processes. The incorporation of these processes into the rate equation model is essential, since the two-photon absorption between 9 and 14 and emission between levels 12 and 6 can seriously influence the lasing performance due to the reduced population inversion between the lasing states 6 and 9. They are taken into account by extending the rate equations system with the rate equation for the density of photons describing single and double-photon stimulated emission processes:

$$\frac{dm_\omega}{dt} = \frac{\Gamma}{d}\left[W_{96}^{p}\left(n_9 - n_6\right) + W_{(14)(12)}^{p}\left(n_{(14)} - n_{(12)}\right) + W_{(12)9}^{p}\left(n_{(12)} - n_9\right)\right] + \\ + 2\frac{\Gamma}{d}\left[W_{(14)9}^{2p}\left(n_{(14)} - n_9\right) + W_{(12)6}^{2p}\left(n_{(12)} - n_6\right)\right] - \frac{m_\omega}{\tau_p^\omega} \tag{4}$$

Here, m_ω is the photon density [m^{-3}], W_{ij}^{p} and W_{ik}^{2p} are the sigle- and double-photon stimulated emission rates, Γ is the mode confinement factor, which is assumed to be 0.5 (Ref. 29), and τ_p^ω is the photon lifetime related to the total loss α_ω as[29] $\tau_p^\omega = \left(v_g \alpha_\omega\right)^{-1}$, where v_g represents the group velocity, $v_g = c/n_\omega$.

The single-photon stimulated emission rate is expressed as[30]:

$$W_{ij}^{p} = \frac{e^2 M_{ij}^2 \omega}{2\varepsilon} \frac{\gamma_{ij}}{\left(E_{ij} - \hbar\omega\right)^2 + \left(\gamma_{ij}/2\right)^2} m_{\omega} \tag{5}$$

where E_{ij} is the energy difference between levels i and j, ε is the permittivity of the lasing medium and ω is the incident photon frequency. It can be seen from the expression [Eq. (5)] that the single-photon stimulated emission rate is proportional to the incident photon density (light intensity). The double-photon stimulated emission/absorption rate in the transition cascade $i - j - k$ is proportional to the photon density squared, as given in Ref. 17, 29:

$$W_{ik}^{2p} = \frac{e^4 M_{ij}^2 M_{jk}^2}{4\hbar\varepsilon^2} \left(\frac{\hbar\omega}{E_{jk} - \hbar\omega} \right) \frac{\gamma_{ik}}{\left(E_{ik} - 2\hbar\omega\right)^2 + \left(\gamma_{ik}/2\right)^2} m^2{}_{\omega} \tag{6}$$

In addition, in the rate equations system described by [Eq. (3)] the total scattering rates between any two levels of the nonlinear cascade in the active region include not only the nonradiative scattering rates, but also the radiative single and two-photon transitions, which are linearly and/or quadratically dependent on the incident photon density.

For transition rates between the adjacent single-photon resonant levels, i.e. W_{69}, W_{96}, $W_{9(12)}$, $W_{(12)9}$, $W_{(12)(14)}$ and $W_{(14)(12)}$ the total transition rate can be expressed as:

$$W_{ij} = W_{ij}^{LO} + W_{ij}^{e-e} + W_{ij}^{p} \tag{7}$$

Similarly, the transition rates between the two-photon resonant levels $W_{6(12)}$, $W_{(12)6}$, $W_{9(14)}$, and $W_{(14)9}$, can now be calculated as:

$$W_{ij} = W_{ij}^{LO} + W_{ij}^{e-e} + W_{ij}^{2p} \tag{8}$$

making the transition rates between the single-photon levels linearly and between the two-photon levels quadratically dependent on the incident photon density. The values for W_{ij}^{p} and W_{ik}^{2p} can be obtained from [Eq. (5)] and [Eq. (6)]. For any other transitions occurring outside the active region, the scattering rates are obtained by taking into account electron-LO

phonon and electron-electron scattering only, making these transitions independent of the photon density in the cavity.

The set of equations expressed by [Eq. (3)], together with [Eq. (4)] describing the photon density, form a total of 16 rate equations whose solution for electron and photon densities n_i and m_ω respectively can enable us to estimate macroscopic parameters of the system, such as the current density or the modal gain. The scattering time $W_{i,f}$ is a function of both n_i and n_f - the initial and final subband populations, as well as the photon density, as stated in [Eq. (5)] and [Eq. (6)], hence the set of equations needs to be solved self-consistently using an iterative procedure Ref. 15, 27.

In this work, the current density flowing through a reference plane placed in the injection barrier of the central period is be calculated using the scattering transport approach, i.e. by subtracting the current density component which is the result of electrons scattering into the next periods of the QCL from the component caused by electrons scattering back, Ref. 15, 27, 28:

$$J = \sum_{k=1}^{P} \sum_{i=1}^{N} \sum_{j=1}^{N} k \cdot n_i \left(W_{i,j+kN} + W_{i+kN,j} \right) \tag{9}$$

Compared to computationally more demanding models, like the density fraction model[31] [32] or the nonequilibrium Green function approach[33] [34] this has proven to be accurate enough in the case of MIR structures.

The factor k in the summation, effective for non-nearest-neighbour scattering, originates from the scatterings from any QCL period left of the central period into any period right of it, or vice versa. Once again, we introduce the "tight-binding" approximation assuming that only the nearest neighbours interact, and set P=2.

The linear and SHG output light intensity can be calculated from the photon density in the cavity as

$$I_\omega = N_{\mathrm{mod}} (\hbar\omega) m_\omega \frac{c}{n_\omega} \tag{10}$$

where N_{mod} is the number of QCL periods in the lasing cavity, and is set to 50 as in Ref. 17 and the factor c/n is the speed of light in the lasing cavity. The output power can now be calculated as:

$$P_\omega = I_\omega A \tag{11}$$

where A represents the cross-sectional area transverse to the light propagation direction.

By solving the steady-state rate equations system given by [Eq. (3)] and [Eq. (4)], we can determine the photon density, and, correspondingly, the initial fundamental power output given by [Eq. (10)] and [Eq. (11)]. The nonlinear output power can then be obtained from the following expression, Ref. 29:

$$P_{2\omega} = \frac{2\pi^2 \left|\chi^{(2)}\right|^2 \left[e^{-2\alpha_{2\varpi} L} - 2e^{-2\alpha_{2\omega} L}\cos(\Delta k L) + 1\right](1-R_2)}{I_R n_\omega^2 n_{2\omega} \lambda^2 c \varepsilon_0 \left(\Delta k^2 + \alpha_{2\omega}^2\right)(1-R_1)^2} P_\omega^2 \tag{12}$$

Here, λ~9μm is the wavelength of the fundamental mode and I_R represents the effective interaction cross section decided by the overlap between the fundamental and the second harmonic mode, which is considered to be equal to the one given in Ref. 17, i.e. 1000μm^2. $n_\omega = k_\omega c/\omega$ and $n_{2\omega} = k_{2\omega} c/\omega$ are refractive indices of the fundamental and second harmonic mode, $\Delta k = 2k_\omega - k_{2\omega}$ the phase constant mismatch and $\alpha_{2\omega}$ is the total loss including both, the waveguide $\alpha^w{}_{2\omega}$ and the mirror loss $\alpha^m{}_{2\omega}$. The waveguide losses, as well as the dimensions of the waveguide are taken from Ref. 17. The mirror losses can be estimated by $\alpha^m_{\omega(2\omega)} = -\left(\ln R_{1(2)}\right)/L$ where L is the cavity length, while R_1 and R_2 are reflection coefficients at the fundamental and second harmonic frequency. They are related to the refractive indices as $R_{1(2)} = \left(1 - n_{\omega(2\omega)}\right)^2 / \left(1 + n_{\omega(2\omega)}\right)^2$.

Changing the bias field modifies the potential experienced by the electrons and consequently the energies and corresponding wave functions of the quasi-bound states. Hence, all the lifetimes and transition matrix elements change, influencing the electric current and, by modifying the subband populations, the gain. By repeating the self-consistent procedure for a number of external fields, macroscopic parameters of the system such as current density and linear and SHG power can be evaluated.

III. NUMERICAL RESULTS AND DISCUSSION

The procedure described above is flexible enough to be applied on a wide variety of structures where a significant number of different operating wavelengths can be tailored. In

this work, we have chosen to address the optimization of the active region for the reference structure described in Ref. 17. It consists of two coupled InGaAs quantum wells separated with an AlInAs barrier, designed for fundamental and SHG wavelengths at λ~9μm and λ~4.5μm, respectively, which sets the fundamental transition energy to approximately 136meV, while the energy difference between the ground and lower laser state equals the LO phonon energy, i.e. 34meV. The optimization was carried out for the value of the applied field of F=38kV/cm, temperature T=10K and the sheet carrier density N_s=37.2x10^{10}cm^{-2}, which was derived from the dopant profile per repeat period and was initially, at the beginning of the self-consistent procedure, assumed to be distributed equally between the subbands of one period.

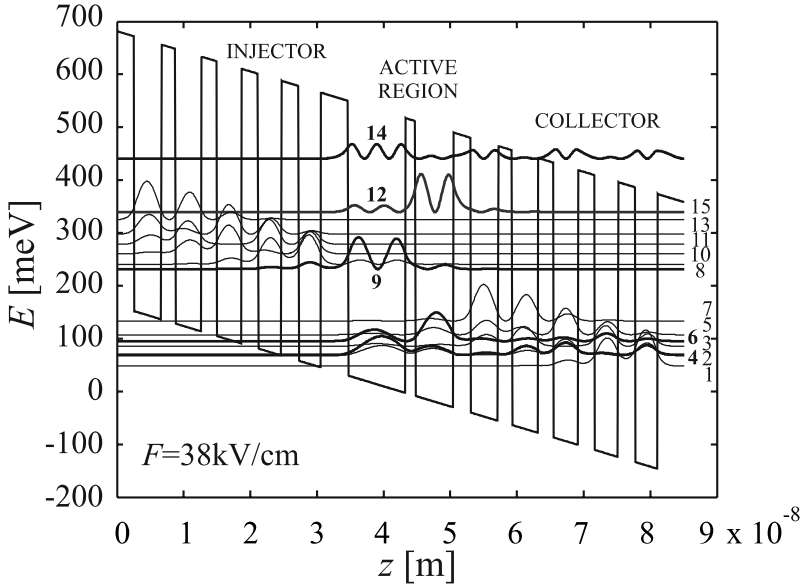

FIG. 2. A schematic diagram of quasi-bound energy levels and associated wave functions squared for one and a half period of the optimized structure. The layer sequence of one period, in nanometers, starting from the injection barrier is: **4.1**, 8.6, **1.5**, 5.7, **2.6**, 4.1, **2.1**, 3.9, **2.3**, 3.7, **2.5**, 3.5, **2.6**, and 3.3. Normal scripts denote the wells and bold the barriers.

A schematic diagram of quasi-bound energy levels and associated wave functions squared for an injector-active region-injector section of the optimized structure is shown in Fig. 2. The layer sequence of one period, in nanometers, starting from the injection barrier is: **4.1**, 8.6, **1.5**, 5.7, **2.6**, 4.1, **2.1**, 3.9, **2.3**, 3.7, **2.5**, 3.5, **2.6**, and 3.3, where normal scripts denote the wells and bold the barriers. The injector and collector regions are represented with five energy levels each, as given in the previous paragraph. The pump radiation at the fundamental frequency is generated between levels 9 and 6. Nonlinear cascades are formed

by levels 6-9-12 and 9-12-14. The first cascade coincides with the laser transition, while the resonance of the second cascade can be achieved by relative thickness variations of the two QWs and the barrier between them. At the applied bias field of 38kV/cm, for which the optimization was performed, the lasing wavelength amounts to λ=9.08μm. Due to the increased overlap between the lasing state wave functions, the optimized structure shows a significant increase of the dipole matrix element, z_{96}=17nm.

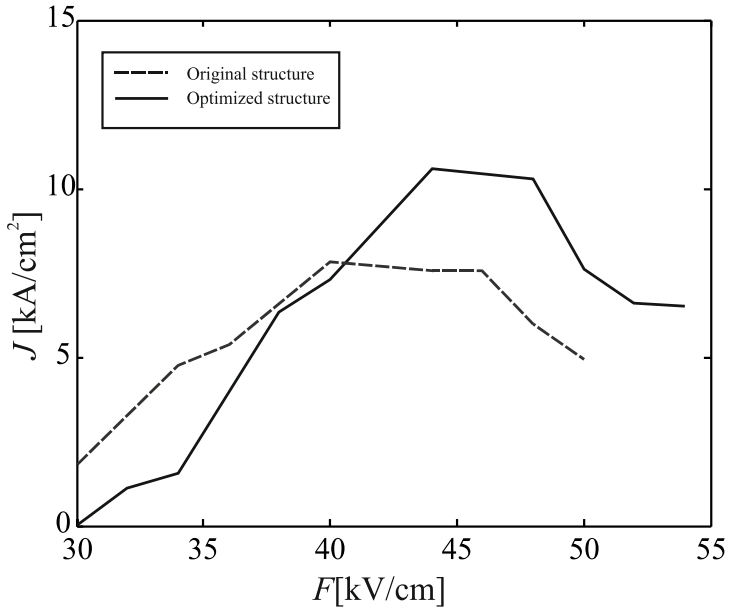

FIG. 3. Electric field vs. current density characteristics at T=10K in the optimized (solid lines) and reference (dashed lines) structure, Ref. 17. The optimized structure shows that higher current densities can be achieved with lower bias fields in the range of applied fields up to 40kV/cm.

By applying the self consistent procedure described in the previous section on both, the reference, Ref. 17, and the optimized structure for T=10K and external field values from 30 to 55kV/cm, the output characteristics were derived and compared. The electric field/current density characteristics are shown in Fig. 3. It can be seen that the optimized structure demonstrates a considerable improvement in that, in a notably wide range of applied fields (above 40kV/cm), higher current densities can be achieved with lower bias fields.

By using [Eq. (13)] and adopting the parameters given in Ref. 17, we can estimate the nonlinear conversion efficiency $\eta=P_{2\omega}/P_{\omega}^{2}$ of 272 μW/W^2 for the reference structure, which is in good agreement with the experimentally obtained values of ~100 μW/W^2 given in Ref. 17. The calculated value for the second order nonlinear susceptibility of $|\chi^{(2)}| = 2.58\times10^4$ pm/V is in accordance with the calculated values of 2×10^4 pm/V given for the reference

structure in Ref. 17. However, the optimized structure shows a noticeable improvement regarding these parameters, and the calculated values for the nonlinear to linear conversion efficiency and the second order nonlinear susceptibility are 349 μW/W^2 and 2.71 ×10^4 pm/V, respectively.

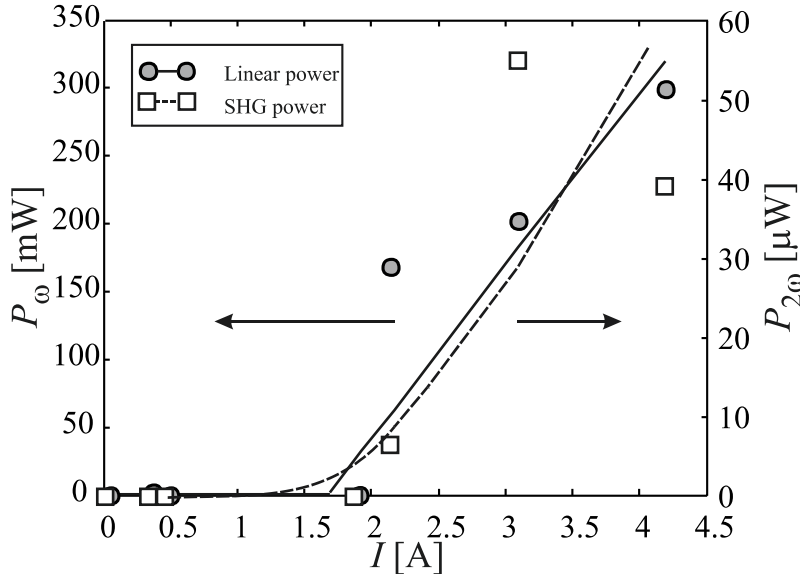

FIG. 4. Fundamental power (straight line) and the nonlinear power (dashed line) under different pump currents for the reference structure. The lines represent interpolated values of the calculated data which is represented by symbols (squares and circles).

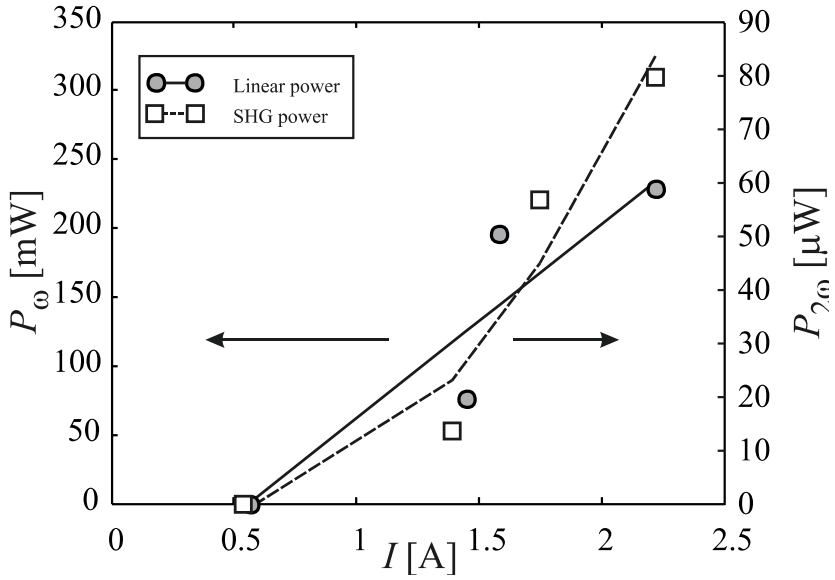

FIG. 5. Fundamental power (straight line) and the nonlinear power (dashed line) under different pump currents for the optimized structure. The lines represent interpolated values of the calculated data which is represented by symbols (squares and circles).

Fig. 4 and Fig. 5 represent the linear and nonlinear output for both the reference and optimized structure. The threshold current estimated for the optimized structure is close to 0.5 A, while the calculated value for the reference structure is about 2 A, which is in good accordance with the experimentally obtained values given in Ref. 17. It can be seen that the optimized structure shows higher linear output powers at lower currents.

As can be seen from the [Eq. (13)], the phase mismatch factor Δk plays a significant role in the nonlinear conversion efficiency estimation. In our calculations, the phase mismatch factor is about 100 times larger than the loss $\alpha_{2\omega}$. Even though the calculated values for the nonlinear conversion efficiency are rather high, they could be additionally enhanced by making the phase mismatch factor comparable to the optical losses, or by decreasing the effective interaction area I_R, which will be the subject of further work.

IV. CONCLUSION

We have described a procedure for the design of a GaInAs-AlInAs-based QCL with optimized optical nonlinearity capability. The technique has no restrictions regarding the number of the optimization parameters or material composition, and demonstrates high optimization abilities. The designs were evaluated by modeling the carrier dynamics using the full self-consistent approach extended with photon density equations, and the reference design calculations show excellent agreement with experimental results. At the same time, the optimzed structure predicts a significant improvement of the nonlinear to linear conversion efficiency and the second order nonlinear susceptibility, as intended. The described procedure is applicable to various active region designs and will be used in further work for other wavelength ranges. The developed method will also be an excellent ground for proper modeling of other higher-order effects in QCLs very relevant for current applications in imaging, spectroscopy and material characterization.

ACKNOWLEDGMENTS

This work was supported by the Ministry of Education, Science and Technological Development (Republic of Serbia), ev.no. III 45010, NATO SfP Grant, ref. no. 984068, and COST Actions BM1205 and MP1204

REFERENCES

[1] B. S. Wlliams, Nat. Photonics, **1**, 517, (2007)

[2] Y. Yao, A. J. Hoffman, and C. F. Gmachl, Nat. Photonics, **6**, 432, (2012)

[3] Y. Petitjean, F. Destic, J. Mollier, and C. Sirtori, IEEE J. Sel. Top. Quantum Electron., **17**, 22, (2011)

[4] F. Capasso, R. Paiella, R. Martini, R. Colombelli, C. Gmachl, T. L. Myers, M. S. Taubman, R. M.Williams, C. G. Bethea, K. Unterrainer, H. Y. Hwang, D. L. Sivco, A. Y. Cho, A. M. Sergent, H. C. Liu, and Edward. A. Whittaker, IEEE J. Quantum Electron., **38**, 511, (2002)

[5] C. Sirtori, P. Kruck, S. Barbieri, P. Collot, J. Nagle, M. Beck, J. Faist, and U. Oesterle, Appl. Phys. Lett. **73**, 3486 (1998)

[6] C. Sirtori, H. Page, and C. Becker, Proc. R. Soc. London, Ser. A **359**, 505 (2001)

[7] S.-C. Lee and A. Wacker, Phys. Rev. B **66**, 245314 (2002)

[8] J. Radovanović, A. Mirčetić, V. Milanović, Z. Ikonić, D. Indjin, P. Harrison, R. W. Kelsall, Semicond. Sci. Technol. **21**, 215, (2006)

[9] S. Höfling, V. D. Jovanović, D. Indjin, J. P. Reithmaier, A. Forchel, Z. Ikonić, N. Vukmirović, P. Harrison, A. Mirčetić, V. Milanović, Appl. Phys. Lett. **88**, 251109, (2006)

[10] M. A. Belkin, F. Capasso, A. Belyanin, D. L. Sivco, A. Y. Cho, D. C. Oakley, C. J. Vineis and G. W. Turner, Nat. Photonics **1**, 288, (2007)

[11] M. A. Belkin, F. Capasso, F. Xie, A. Belyanin, M. Fischer, A. Wittmann, and J. Faist, Appl. Phys. Lett. **92**, 201101, (2008)

[12] J.-Y. Bengloan, A. De Rossi, V. Ortiz, X. Marcadet, M. Calligaro, I. Maurin and C. Sirtori, Appl. Phys. Lett. **84**, 2019, (2004)

[13] Y. R. Shen, *The Principles of Nonlinear Optics*, (Wiley, New York, 1984).

[14] O. Malis, A. Belyanin, C. Gmachl, D. L. Sivco, M. L. Peabody, A. M. Sergent, and Alfred Y. Cho, Appl. Phys. Lett. **84**, 2721, (2004)

[15] A. Mirčetić, D. Indjin, Z. Ikonić, P. Harrison, V. Milanović, R. W. Kelsall, J. Appl. Phys. **97**, 084506, (2005).

[16] B. Novaković, J. Radovanović, A. Mirčetić, V. Milanović, Z. Ikonić, D. Indjin, Opt. Comm. **279**, 330, (2007).

[17] C. Gmachl, A. Belyanin, D. L. Sivco, M. L. Peabody, N. Owschimikow, A. M. Sergent, F. Capasso, and A. Y. Cho, IEEE J. Quantum Electron. **39**, 1345, (2003).

[18] A Hugi, R Maulini, J. Faist, Semicond. Sci. Technol., **25**, 083001, (2010)

[19] Y Petitjen, F Destic, J-C Mollier, C Sirtori, J. Sel. Top. Quantum Electron., **17**, 22, (2011)

[20] D. E. Goldberg, *Genetic Algorithms in Search, Optimization and Machine Learning*, (Addison-Wesley, Boston, 1989)

[21] David L. Carroll, University of Illinois, 306 Talbot Lab, 104 S. Wright St., Urbana, IL 61801

[22] C. Gmachl, F. Capasso, D. L. Sivco, and A. Y. Cho, Rep. on Progress in Physics, **64**, 1533, (2001).

[23] J. Bai, D. S. Citrin, Opt. Express, **14**, 4043, (2006).

[24] P. Dean, Y. L. Lim, A. Valavanis, A. R. Kliese, M. Nikolić, S. P. Khanna, M. Lachab, D. Indjin. Z Ikonić, P. Harrison, A. D. Rakić, E. H. Linfield, and A. G. Davies, Opt. Lett., **36**, 2587, (2011)

[25] A. Daničić, J. Radovanović, V. Milanović, D. Indjin, and Z. Ikonić, J. Phys. D: Appl. Phys., **43**, 045101, (2010)

[26] Y. L. Lim, P. Dean, M. Nikoli, R. Kliese, S. P. Khanna, M. Lachab, A. Valavanis, D. Indjin, Z. Ikonić, P. Harrison, E. H. Linfield, A. G. Davies, S. J. Wilson, and A. D. Rakić, Appl. Phys. Lett., **99**, 081108, (2011)

[27] D. Indjin, P. Harrison, R. W. Kelsall, and Z. Ikonić, J. Appl. Phys. **91**, 9019 (2002)

[28] V. D. Jovanović, S. Höfling, D. Indjin, N. Vukmirović, Z. Ikonić, P. Harrison, J. P. Reithmaier, and A. Forchel, J. Appl. Phys. **99**, 103106, (2006)

[29] J. Bai, D. S. Citrin, J. Quantum Electron., **43**, 391, (2007)

[30] R. W. Boyd, Nonlinear Optics, 2nd ed. San Diego, CA: Academic, 528, (2003).

[31] G. Beji, Z. Ikonić, C. A. Evans, D. Indjin, and P. Harrison, J. Appl. Phys., **109**, (2011)

[32] E. Dupont, S. Fathololoumi, and H. C. Liu, Phys. Rev. B, **81**, 205311, (2010)

[33] N. Vukmirović, D. Indjin, Z. Ikonić, and P. Harrison, IEEE Phot. Technol. Lett., **20**, 129, (2008)

[34] A. Wacker, M. Lindskog, and D. O. Winge, IEEE J. Sel. Top. Quantum Electron., **19**, 1200611, (2013)